



RESEARCH LETTER

10.1002/2015GL066784

Key Points:

- A new method for quantifying lava dome growth from SAR amplitude features
- The dome of Mount Cleveland grew upward by more than 60 m in August 2011
- The dome grew from an open-conduit magmatic system without deforming the crust

Supporting Information:

- Texts S1 and S2, Figures S1–S6, and Table S1
- Figure S1
- Figure S2
- Figure S3
- Figure S4
- Figure S5
- Figure S6

Correspondence to:

T. Wang,
teng.wang@kaust.edu.sa

Citation:

Wang, T., M. P. Poland, and Z. Lu (2015), Dome growth at Mount Cleveland, Aleutian Arc, quantified by time series TerraSAR-X imagery, *Geophys. Res. Lett.*, 42, doi:10.1002/2015GL066784.

Received 27 OCT 2015

Accepted 3 DEC 2015

Accepted article online 9 DEC 2015

Dome growth at Mount Cleveland, Aleutian Arc, quantified by time series TerraSAR-X imagery

Teng Wang¹, Michael P. Poland², and Zhong Lu¹

¹Huffington Department of Earth Sciences, Southern Methodist University, Dallas, Texas, USA, ²Cascades Volcano Observatory, U.S. Geological Survey, Vancouver, Washington, USA

Abstract Synthetic aperture radar imagery is widely used to study surface deformation induced by volcanic activity; however, it is rarely applied to quantify the evolution of lava domes, which is important for understanding hazards and magmatic system characteristics. We studied dome formation associated with eruptive activity at Mount Cleveland, Aleutian Volcanic Arc, in 2011–2012 using TerraSAR-X imagery. Interferometry and offset tracking show no consistent deformation and only motion of the crater rim, suggesting that ascending magma may pass through a preexisting conduit system without causing appreciable surface deformation. Amplitude imagery has proven useful for quantifying rates of vertical and areal growth of the lava dome within the crater from formation to removal by explosive activity to rebirth. We expect that this approach can be applied at other volcanoes that host growing lava domes and where hazards are highly dependent on dome geometry and growth rates.

1. Introduction

Ground deformation at volcanoes is an important indicator of what is happening beneath the surface and has been monitored using synthetic aperture radar (SAR) interferometry (InSAR) at many volcanoes [e.g., Lu and Dzurisin, 2014; Pinel et al., 2014; Biggs et al., 2014]. Mechanisms for volcano deformation as deduced from InSAR include magma accumulation and withdrawal [e.g., Lu et al., 2010], faulting [e.g., Amelung et al., 2000], dyke intrusion, [e.g., Wicks et al., 2011], and edifice instability [e.g., Schaefer et al., 2015]. In addition to studies that map deformation from single or small numbers of interferograms, time series InSAR techniques have been used to great effect at many volcanoes to estimate such parameters as lava volume [Lu et al., 2003; Poland, 2014] and long-term deformation associated with magmatic recharge [e.g., Hooper et al., 2004; Puglisi et al., 2008]. While SAR and InSAR are commonly applied to quantify volcano-wide deformation and eruptive activity, they are less frequently used to study lava dome emplacement, even though the process is relatively common. This is due to the small spatial extent of many lava domes, as well as the tendency for domes to be incoherent in InSAR imagery over relatively short timescales (days to months). A noteworthy example of the value in SAR data for tracking lava dome growth is that of Merapi, Indonesia, in 2010, where amplitude imagery aided in the recognition of rapid dome growth and assessment of collapse potential despite persistent cloud cover that obscured other types of observations (especially at visible wavelengths) [Pallister et al., 2013]. Tracking dome growth and deformation (both of the dome and surrounding terrain) is critical for hazards assessment because dome growth rate has been tied to explosive potential [e.g., Pallister et al., 2013], and localized transient deformation has been shown to immediately precede explosions at some dome-building volcanoes [e.g., Salzer et al., 2014].

In situ cameras installed near a volcano's summit can provide some of the necessary data to assess dome growth and deformation, as demonstrated at Merapi [Walter et al., 2013a], Colima, Mexico [Walter et al., 2013b], Soufrière Hills, Montserrat [Herd et al., 2005], and Mount St. Helens, U.S. [Major et al., 2009], but the method is fraught with challenges. Few volcanoes have geometries conducive to camera placement, instrument maintenance can be hazardous, and inclement weather frequently occludes views of the dome. We undertake a detailed analysis of dome growth at Cleveland volcano in the Aleutian Arc of Alaska using SAR imagery. While we do examine InSAR results for signs of deformation of the volcano, our primary focus is on SAR amplitude data, which are often overlooked in deference to interferograms for volcano monitoring and research applications. The rich information in these images allows us to track dome growth at Cleveland over time, including a quantification of dome area and height, which together provide a means of estimating effusion rate. Such data represent critical information for hazards assessment at dome-building volcanoes.

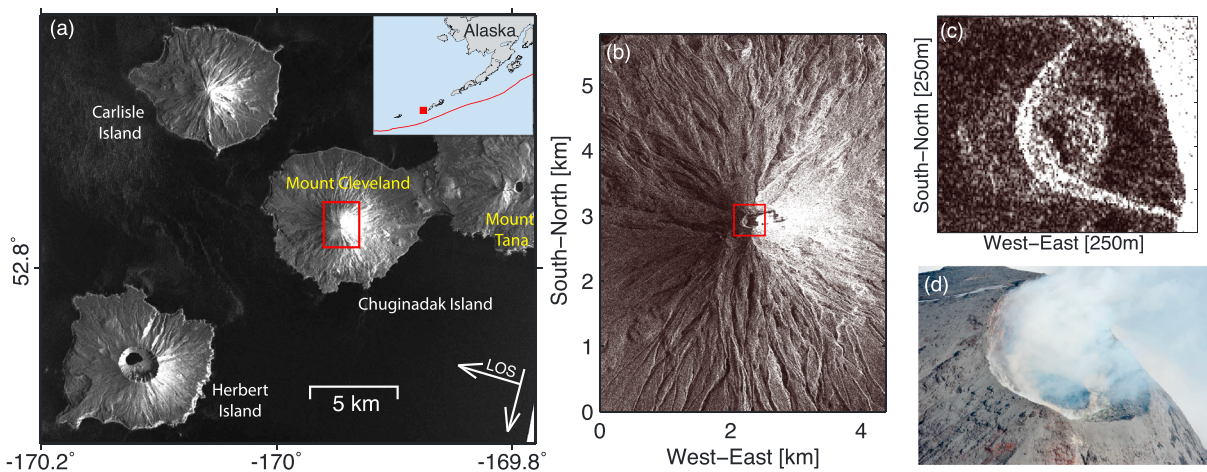


Figure 1. TerraSAR-X amplitude image acquired on 7 August 2011. (a) The amplitude image of Carlisle, Herbert, and Chuginadak Islands, the latter of which is composed by Mount Cleveland and Mount Tana. Inset shows the location of Mount Cleveland in the Aleutian Arc, with red line representing the Aleutian trench. (b and c) The detailed georeferenced images of Mount Cleveland and its summit crater. Note that the georeferencing of the top of Mount Cleveland is not precise as we do not have a high-resolution DEM reflecting the crater structure. (d) The volcano's crater and growing lava dome are visible in a photo taken on 8 August 2011, from an airplane operated by Alaska Volcano Observatory scientists (<https://www.avo.alaska.edu/images/image.php?id=36192>).

2. Background

Mount Cleveland (1730 m above sea level, asl) is located in the east central Aleutians on the western half of the uninhabited Chuginadak Island (Figure 1) and is one of the most frequently active volcanoes in the arc [Miller *et al.*, 1998; Lu and Dzurisin, 2014]. Especially noteworthy eruptive activity occurred in February 2001, when three explosive events produced ash clouds as high as 12 km, threatening aviation. Rubbly lava flows, a hot avalanche, and several lahars were also produced in the eruption, some of which reached the sea [Dean *et al.*, 2004]. Analysis of Envisat-advanced synthetic aperture radar (ASAR), Advanced Land Observing Satellite-1-Phased Array type L-band Synthetic Aperture Radar (ALOS-1 PALSAR), and Uninhabited Aerial Vehicle Synthetic Aperture Radar (UAVSAR) data indicates that there has been no significant deformation of the volcano since at least the early 2000s. Lu and Dzurisin [2014] concluded that Mount Cleveland is an open-conduit system where eruptions occur frequently without deforming the surface. This conclusion is uncertain, however, because the slope near the summit area is greater than 40°, making it a challenging site for any SAR/InSAR analysis surrounding the crater area.

The following account of Mount Cleveland's 2011–2012 eruptive activity is drawn from McGimsey *et al.* [2014] and Herrick *et al.* [2014], as well as personal communications with Alaska Volcano Observatory (AVO) scientists. On 16–17 July 2011, AVO observed thermal anomalies in satellite data covering Mount Cleveland. A few days later, on 31 July, satellite imagery revealed a small lava dome about 40 m in diameter in the summit crater. The dome is also clearly visible in the TerraSAR-X image acquired on 7 August and photos from 8 August (Figures 1c and 1d). As the most recent clear optical image of the summit area from 7 July did not show any lava dome, AVO suggested that dome extrusion began at about the time of the observed thermal anomalies. Lava extrusion continued intermittently in the weeks that followed, effectively filling the crater, until dome growth apparently paused in early October. A smaller dome began growing atop the existing dome in early November, but extrusion occurred over only a few days, and the smaller dome was no longer distinguishable by early December. During this entire sequence of dome emplacement, no significant ash emissions were detected, and accumulation of lava was confined to the summit crater.

On 29 December 2011, an ash cloud was detected at 3500 m asl in satellite images of Mount Cleveland as a consequence of an explosion that occurred at approximately 13:12 UTC. The explosion was detected by seismic and infrasound stations located 140 km NE of the volcano, and subsequent analysis of satellite and infrasound data revealed the occurrence of smaller explosions on 25 December as well [Angelis *et al.*, 2012]. The lava dome that formed during fall to winter 2011 was largely removed by the explosive activity, and no new lava was extruded for over a month until a new ~40 m diameter dome was detected in satellite

data from 30 January 2012. Dome growth continued into early March, when a series of explosions removed the dome again by 11 March. Several additional cycles of dome growth and explosions continued throughout much of the remainder of 2012 and were detected by seismic, infrasound, and satellite data [Angelis *et al.*, 2012].

2.1. SAR Data and InSAR Observations

A total of 10 stripmap mode X-band TerraSAR-X descending track SAR images were acquired of Mount Cleveland between 7 August 2011 and 8 January 2012, and two high-resolution spotlight images were collected on 19 January and 10 February 2012. The satellite look direction was to the west along an incidence angle of about 36° from the vertical, with a pixel spacing of 2 m in azimuth and 0.9 m in range (ground pixel spacing of 1.5 m) for stripmap images and 0.86 m in azimuth and 0.45 m in range (ground pixel spacing of 0.75 m) for spotlight images.

We formed differential interferograms between all the images [Wang *et al.*, 2014], and despite the overall good coherence of these interferograms no consistent patterns of deformation were apparent on Mount Cleveland (see supporting information Text S1 and Figures S1–S3). This observation is consistent with previous studies, which concluded that magma at Cleveland may ascend through an open conduit without producing large-scale surface deformation [Lu and Dzurisin, 2014]. We then focused on the summit area to analyze whether or not any localized displacements occurred during eruptive activity in 2011–2012 (Figure S4). Patches with different phase values can be observed from the two coherent interferograms spanning August 2011, demonstrating that the crater rim deformed during extrusion of the dome. However, phase unwrapping was not practical as the localized deformation between adjacent moving targets on the crater rim may be larger than half of the wavelength (~ 1.5 cm) during dome emplacement. The dome surface was completely decorrelated.

3. Quantifying Dome Growth by Tracking Features in SAR Amplitude Images

3.1. TerraSAR-X Amplitude Images

The features in SAR amplitude images result from the scattering characteristics of the surface and the SAR imaging geometry. Bright pixels in the near-range part of upper flanks, just below the rim on the east side of the volcano, are caused by foreshortening in SAR images—that is, this part of the flank faces the satellite, reflecting more energy back to the radar (Figures 1 and 2). The far-range part of the upper flanks and crater, on the west side of the volcano, is characterized by a bright edge due to the strong reflectivity of rocks on the crater rim, surrounded by areas both within and outside of the crater that have weaker returns because they slope away from the satellite's look direction. Starting with the first TerraSAR-X image in the sequence (acquired on 7 August 2011), a lava dome can be clearly distinguished from the dark background because of the rough, and therefore bright, surface of the newly erupted lava, which reflects more energy back to the radar. It is also interesting to observe a small dark patch in the middle of the dome in the three amplitude images acquired in August, suggesting a relatively smooth top to the dome, similar to what was observed at the volcano in 2015 (<http://www.avo.alaska.edu/images/dbimages/display/1439229412.jpg>).

Paradoxically, reflectors associated with the lava dome appear outside the crater area, to the west, in the far range of the radar, in the earliest images of the sequence (7, 18, and 29 August 2011; Figures 1c and 2). This is caused by the fact that the dome is lower than the crater rim, so reflections from the dome take longer to be received at the satellite than those from the crater rim—an effect referred to as layover. Portions of the dome therefore appear to occur outside the crater until dome growth was sufficient to raise the level of the dome closer to that of the rim. This condition was met by the time of the 9 September 2011 image. Dome growth is also manifested by an apparent right (far range) to left (near range) migration of the dome from 29 August to 3 November. After 12 October 2011, the dome fully filled the crater, as indicated by the lack of distinction between the boundaries of the crater rim and the dome in the image acquired on 23 October. The dome was not present in the image acquired on 8 January 2012, reflecting removal of the dome by the explosions of late December 2011 [Angelis *et al.*, 2012]. A new dome was evident in the spotlight mode image acquired on 10 February 2012.

Based on the scattering characteristics of the crater rim and the dome, we are able to distinguish bright pixels (red and yellow crosses in Figure 2, top left) from the background [Wang and Jónsson, 2015]. As InSAR cannot

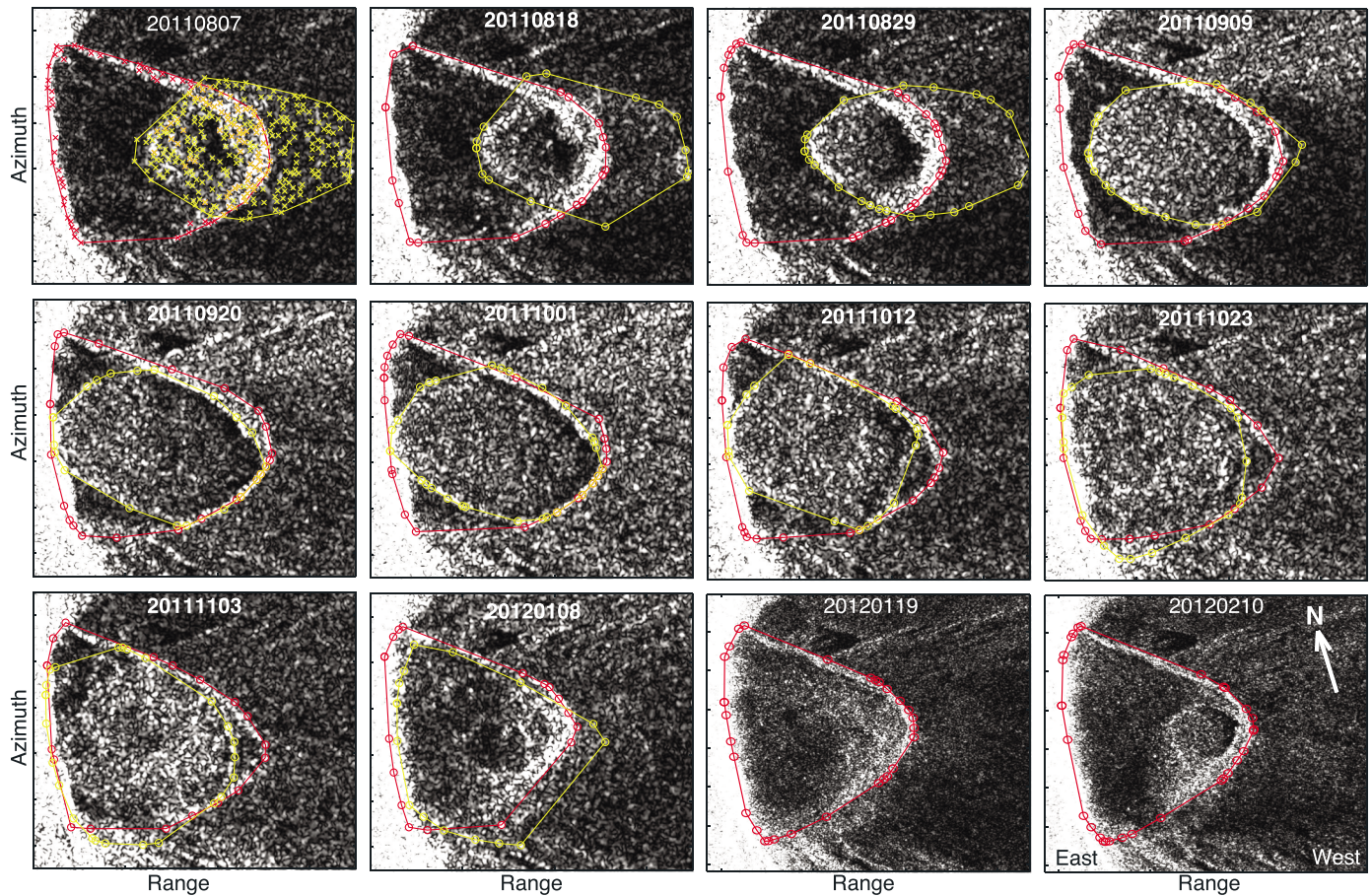


Figure 2. Time series of TerraSAR-X amplitude images focused on the summit area of Mount Cleveland. All the images are oversampled by factors of 4 in azimuth and range directions. The small yellow crosses in the top left plate indicate strong reflectors on the top of the dome. Red and yellow lines in all images are bounding polygons denoting the areas covered by the crater rim and dome, respectively. Note that these images are displayed in radar coordinates; therefore, north is not exactly toward the top of the image, and east and west are reversed. The extent of each image is about 250 m by 250 m.

retrieve the direction of the motion on the crater rim due to phase ambiguity, we performed pixel offset tracking on the detected strong scatterers, estimating offsets in the azimuth and range directions from the peak location of the cross-correlation surface. These offsets only revealed very localized displacements, probably due to the instability of rocks on the crater rim during the growth of the lava dome (see Text S2 and Figure S5). In the following sections, we will focus on quantifying the dome growth from feature tracking and SAR imaging geometry.

3.2. SAR Imaging Geometry for Crater Structure

SAR has an oblique slant-range imaging geometry in which the sensor-to-target distance determines the location of a pixel along a range line. Targets imaged in the near-range position have shorter sensor-to-target distance than targets imaged in the far range. The elevation change dh over time of a target in SAR images with an incidence angle θ can be obtained from the slant-range position change dr :

$$dh = \frac{dr}{\cos \theta} \quad (1)$$

Based on the strong reflectors detected in the amplitude images, we are able to determine the shape and motion of the dome by calculating its bounding polygons and geometric centers.

To test our ability to track dome growth over time using this relation, we constructed a synthetic crater and lava dome structure by reducing the elevation of the summit of the Cleveland digital elevation model (DEM)

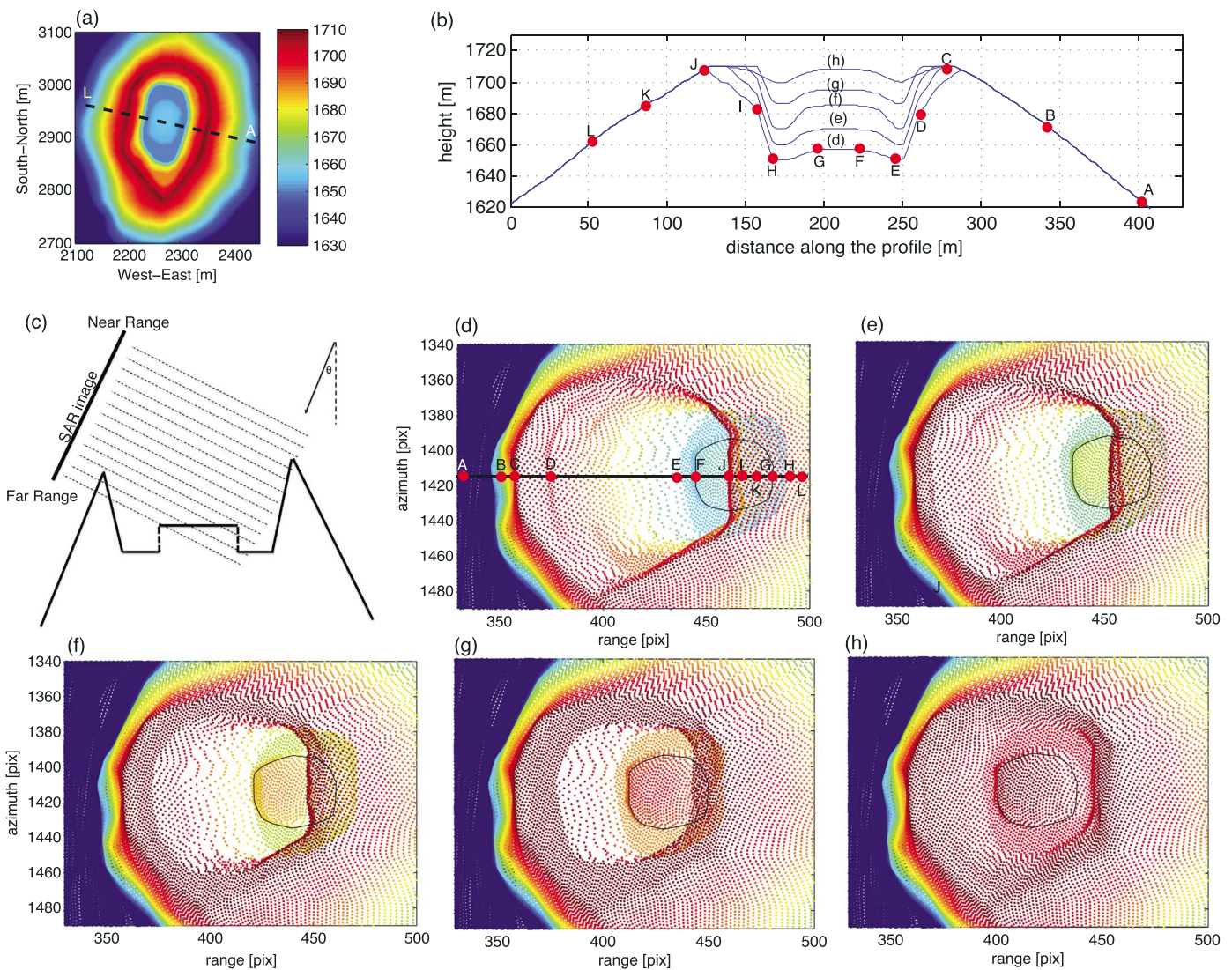


Figure 3. Simulation of SAR imagery for a growing dome inside a crater. (a) Artificial DEM representing topography of the crater and the uppermost flanks of Mount Cleveland. (b) DEM profile (dashed line in Figure 3a) used to project the locations of the scatterers from the crater area into SAR images over time. (c) Sketch of SAR imaging geometry. The pixel locations from near range to far range depend on their slant-range distances to the satellite. (d–h) Projection of scatterers in the DEM to SAR images while the dome (outlined by black line) is uplifted by 10 m in each step. Due to the slant-range imaging geometry, the scatterers on the ground are distorted in the SAR image due to variations of their elevations (compare positions of points A–L in Figures 3b and 3d).

and adding a round dome on the bottom (Figures 3a and 3b). We then progressively uplifted the dome from 50 m below the rim until the top of the dome is at the same elevation as the rim, projecting each point from the artificial DEM into SAR coordinates at each step using the orbital and geometric parameters of the TerraSAR-X imagery (Figures 3d–3h). The simulation demonstrates that the backscattering returns from the dome appear outside the crater in the SAR image (Figures 3d–3f) when the dome has larger slant-range distance than the crater rim, which occurs during the early stages of dome growth. As the dome grows upward, it shifts from near range to far range, appearing more toward the center of the crater. When the dome fills the crater, i.e., the dome top is only slightly lower than the crater rim, the backscattering of the dome appears inside the crater in a SAR image (Figure 3h). Based on this simulation, we conclude that the dome top is at about the level of the crater rim in images acquired during September–December 2011. The new dome of February 2012, which began growing after the destruction of the previous dome in December 2011, also appears toward the center of the crater (Figure 2, lower right), suggesting that the crater floor was

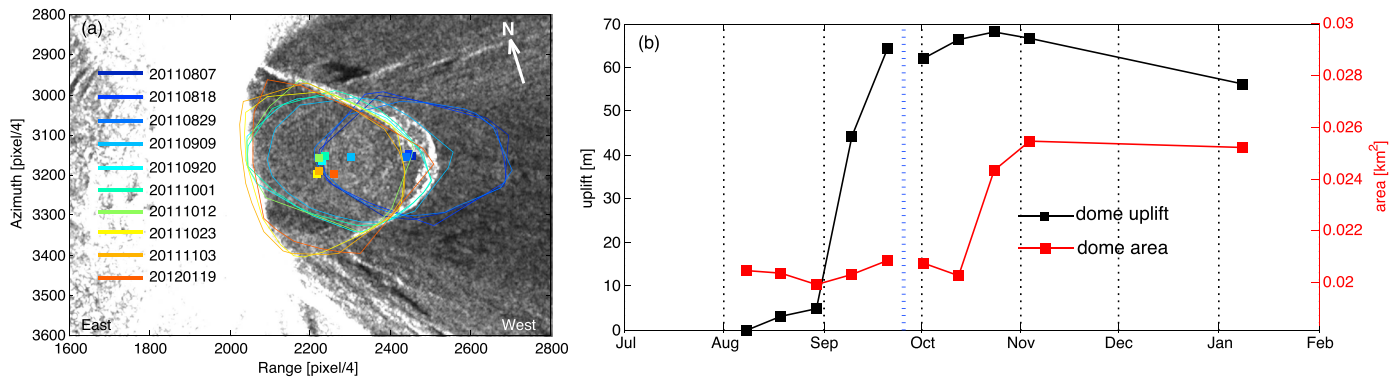


Figure 4. The growing dome detected from features in SAR amplitude images. (a) Bounding polygons of the growing dome along with their geometric centers indicated as color-coded squares. The background is the SAR amplitude averaged over the time period spanned and oversampled by a factor of 4. (b) Vertical growth and area of the dome at the times of SAR acquisitions. The blue dashed line indicates the overlapping of the crater rim and dome edge in the SAR image, causing a discontinuity in uplift and area measurements.

already at a high level compared to August 2011. The early 2012 crater may have been filled with the debris of the previous dome, providing a high platform on which the new dome grew.

3.3. Dome Growth Quantified From Feature Tracking

As mentioned before, the surface scattering characteristics on the dome surface varied rapidly during extrusion, and we are therefore not able to retrieve reliable phase change or pixel offsets from within the crater. With knowledge of SAR imaging geometry, however, our dome growth simulation (Figure 3) demonstrates that we can quantify the vertical growth of the dome by determining range changes of the geometric centers derived from the detected bright scatterers over time using equation (1) (Figure 4). This approach assumes that all slant-range changes are due to vertical growth of the dome, which is likely given that domes at Cleveland are roughly symmetrical (Figure 1d and photo referenced in section 3.1) and grow within the confines of a crater. We can detect horizontal spreading of the dome by mapping its area. As long as it grows radially and not asymmetrically, the range offset of the geometric center in the SAR image would still indicate vertical motion. By assuming an ellipsoidal shape for the dome, we can use the area and height changes to estimate an epoch-to-epoch lava discharge rate for the dome after the time of its initial emplacement (see supporting information Figure S6 and Table S1). Volume changes should be considered minimums, since an ellipsoidal shape will yield a slightly smaller volume than, for example, a cylindrical, pancake-like shape.

As shown in Figure 4a and Table S1, from 7 August to 29 August 2011, the dome moved about 15 pixels (3.8 m) from the far range to the near range, meaning that it grew upward by about 4.7 m (a discharge rate of $\sim 0.04 \text{ m}^3/\text{s}$). From 29 August to 9 September, it grew by about 40 m vertically and from 9 to 20 September by about 20 m, with discharge rates of $\sim 0.6 \text{ m}^3/\text{s}$ and $\sim 0.3 \text{ m}^3/\text{s}$, respectively. We were not able to estimate the elevation changes between images acquired on 20 September and 1 October, as the dome edge in the near range is indistinguishable from the crater rim (Figure 2). Nevertheless, we can separately track the vertical growth of the dome after September, assuming that this indistinguishable edge of the dome did not change much in images acquired after September 20. The result shows that the dome continued to move upward in October at a rate similar to that in August (about 0.3 m/day) (Figure 4b).

To test our assumption of vertical motion, we calculated the area of the bounding polygons in a local universal transverse Mercator coordinate system. By geocoding the images, we updated the initial elevation of the detected bright scatterers based on the uplift calculated from tracking the geometric centers of the dome. The areas of bounding polygons are consistent over time, and the geometric center moves along the range direction in SAR images until October 12, indicating that motion depicted is mainly vertical. After this time, the significant increase in the areal extent of detected strong reflectors probably indicates some lateral spreading of the dome (Figure 4b, red line). Note that the uplift estimation after

12 October may not be reliable because the shape of the dome changed significantly due to spreading, violating the assumption that the indistinguishable edge did not change.

4. Discussion and Conclusions

Aleutian volcanoes have been systematically studied by analyzing tens of thousands of C-, L-, and X-band SAR images acquired from the early 1990s to 2010s [Lu and Dzurisin, 2014]. Results show that a few volcanoes located in the central part of the arc, including Mount Cleveland, erupt frequently without associated surface deformation. Our TerraSAR-X InSAR results from Cleveland's 2011–2012 dome emplacement episodes are consistent with data spanning previous eruptive activity and confirm the continued lack of significant volcano-wide coeruptive deformation. Possible reasons for this lack of surface motion include that deformation cancels out over the time, any magma storage may occur too deep or too shallow to cause detectable deformation, or magma may ascend through an open conduit [Moran *et al.*, 2006]. We cannot rule out that magma accumulation and withdrawal may occur too deep to be detected by InSAR. Indeed, volcano-wide deformation associated with dome extrusion at Mount St. Helens, Washington, during 2004–2005 was broad and small in magnitude [Poland and Lu, 2008]; similar surface motions may not be detectable at Mount Cleveland given the small scale of the island and large magnitude of atmospheric artifacts (Figure S2). In addition, the first TerraSAR-X image was acquired after the appearance of the new dome, so we cannot exclude the possibility that deformation occurred prior to or during the onset of dome extrusion, although no significant deformation was evident over the course of the extrusion during late 2011, including the period of most rapid growth in September. We can, however, largely discount shallow magma storage directly beneath the crater as an explanation for the lack of deformation at Mount Cleveland. The high-resolution TerraSAR-X data preserve some coherence in the summit region, where phase changes and pixel offsets are not consistent with a shallow subsurface source of pressure change (although we cannot exclude the possibility of hours-long cycles of near-field deformation, as observed at some dome-building volcanoes [e.g., Voight *et al.*, 1999]). On the basis of these results, we agree with previous work that Mount Cleveland and similar Aleutian volcanoes (like Shishaldin) are not characterized by significant deformation related to magma accumulation and withdrawal, most likely because their open conduits provide pathways for magma ascent without straining the surface.

Of more value than InSAR observations at Cleveland for tracking changes in eruptive activity, and especially dome formation and evolution, is SAR amplitude data. Lava dome collapse represents a significant hazard at many volcanoes worldwide and has been responsible for large numbers of fatalities [Fink and Anderson, 2000], and the potential for collapse can be assessed by monitoring dome growth rates and morphology [Griffiths and Fink, 1997]. Because volcanic summits, where domes frequently form, are often obscured from visual observations by cloud cover, SAR data fill a vital monitoring niche. Indeed, SAR amplitude images were critical for tracking lava dome growth at Merapi in 2010 and were used to accurately forecast times of increased potential for collapse—forecasts that probably saved thousands of lives [Pallister *et al.*, 2013]. SAR amplitude data have also been used to measure deposition rates of pyroclastic flows at Soufrière Hills volcano, which was important for quantifying flow volumes and constraining magma budgets [Wadge *et al.*, 2011]. Using knowledge of the SAR imaging geometry at Mount Cleveland, we retrieved the rate of vertical dome growth over time, which allowed us to estimate lava discharge rates. These data revealed that the dome was emplaced episodically, occasionally reaching vertical growth rates of several meters per day but with maximum time-averaged lava discharge rates of no more than $0.6 \text{ m}^3/\text{s}$ —very low compared to the most hazardous lava dome eruptions [e.g., Pallister *et al.*, 2013]. As the dome filled the crater, pressure on the conduit must have increased considerably, slowing dome growth and possibly motivating the December 2011 explosive activity that resulted in dome removal [e.g., Voight and Elsworth, 2000]. The 2011 sequence is typical of activity at Mount Cleveland: the January 2012 dome was destroyed by a series of explosions in March 2012, and such cycles were repeated several times during the rest of 2012 and into 2013. Routine acquisition of high-resolution SAR imagery is critical for monitoring dome growth cycles at Mount Cleveland and elsewhere. Such data have the capacity to capture localized preeruption deformation should it occur, and, perhaps more importantly, the imagery can quantify dome growth rates over time regardless of weather conditions. SAR amplitude data may therefore be used to identify periods of heightened potential for explosions and collapse—information vital for hazards assessment and mitigation efforts not only for ground-based populations but also for aviation traffic.

Acknowledgments

The presented dome parameters are available in supporting information Table S1; any additional data may be obtained from T.W. (tengw@smu.edu). The TerraSAR-X data are copyrighted by German Aerospace Center (DLR) 2011–2012 and were provided through GEO1088. The reported research was supported by NASA Earth Surface & Interior Program grant NNX14AQ95G (T.W. and Z.L.), USGS Volcano Hazards Program (M.P.), and the Shuler-Foscue Endowment at Southern Methodist University (Z.L.). We thank Geoff Wadge, Rick Wessels, Daniel Dzurisin, and one anonymous reviewer for their constructive comments.

References

- Amelung, F., S. Jónsson, H. Zebker, and P. Segall (2000), Widespread uplift and “trapdoor” faulting on Galápagos volcanoes observed with radar interferometry, *Nature*, 407(6807), 993–996, doi:10.1038/35039604.
- Angelis, S., D. Fee, M. Haney, and D. Schneider (2012), Detecting hidden volcanic explosions from Mt. Cleveland Volcano, Alaska with infrasound and ground-coupled airwaves, *Geophys. Res. Lett.*, 39, L21312, doi:10.1029/2012GL053635.
- Biggs, J., S. K. Ebmeier, W. P. Aspinall, Z. Lu, M. E. Pritchard, R. S. J. Sparks, and T. A. Mather (2014), Global link between deformation and volcanic eruption quantified by satellite imagery, *Nat. Commun.*, 5, 3471, doi:10.1038/ncomms4471.
- Dean, K., J. Dehn, K. Papp, S. Smith, P. Izbekov, R. Peterson, C. Kearney, and A. Steffke (2004), Integrated satellite observations of the 2001 eruption of Mt. Cleveland, Alaska, *J. Volcanol. Geotherm. Res.*, 135(1–2), 51–73, doi:10.1016/j.jvolgeores.2003.12.013.
- Fink, J. H., and S. W. Anderson (2000), Lava domes and coulees, in *Encyclopedia of Volcanoes*, edited by H. Sigurdsson, pp. 307–319, Academic Press, San Diego, Calif.
- Griffiths, R. W., and J. H. Fink (1997), Solidifying Bingham extrusions: A model for the growth of silicic lava domes, *J. Fluid Mech.*, 347, 13–36.
- Herd, R. A., M. Edmonds, and V. A. Bass (2005), Catastrophic lava dome failure at Soufrière Hills Volcano, Montserrat, 12–13 July 2003, *J. Volcanol. Geotherm. Res.*, 148(3–4), 234–252.
- Herrick, J. A., C. A. Neal, C. E. Cameron, J. P. Dixon, and R. G. McGimsey (2014), Volcanic activity in Alaska: Summary of events and response of the Alaska Volcano Observatory, *U.S. Geol. Surv. Sci. Invest. Rep.*, 2014-5160, 82 p.
- Hooper, A., H. Zebker, P. Segall, and B. Kampes (2004), A new method for measuring deformation on volcanoes and other natural terrains using InSAR persistent scatterers, *Geophys. Res. Lett.*, 31, L23611, doi:10.1029/2004GL021737.
- Lu, Z., and D. Dzurisin (2014), *InSAR Imaging of Aleutian Volcanoes: Monitoring a Volcanic Arc From Space*, Geophys. Sci., 390 pp., Springer Praxis Books, Berlin.
- Lu, Z., E. Fielding, M. Patrick, and C. Trautwein (2003), Estimating lava volume by precision combination of multiple baseline spaceborne and airborne interferometric synthetic aperture radar: The 1997 eruption of Okmok Volcano, Alaska, *IEEE Trans. Geosci. Remote Sens.*, 41(6), 1428–1436, doi:10.1109/TGRS.2003.811553.
- Lu, Z., D. Dzurisin, J. Biggs, C. Wicks, and S. McNutt (2010), Ground surface deformation patterns, magma supply, and magma storage at Okmok Volcano, Alaska, from InSAR analysis: 1. Interruption deformation, 1997–2008, *J. Geophys. Res.*, 115, B00B02, doi:10.1029/2009JB006969.
- Major, J. J., D. Dzurisin, S. P. Schilling, and M. P. Poland (2009), Monitoring lava-dome growth during the 2004–2008 Mount St. Helens, Washington, eruption using oblique terrestrial photography, *Earth Planet. Sci. Lett.*, 286(1–2), 243–254, doi:10.1016/j.epsl.2009.06.034.
- McGimsey, R. G., J. Z. Maharrey, and C. A. Neal (2014), Volcanic activity in Alaska: Summary of events and response of the Alaska Volcano Observatory, *U.S. Geol. Surv. Sci. Invest. Rep.*, 2014-5159, 50 p.
- Miller, T. P., R. G. McGimsey, D. H. Richter, J. R. Riehle, C. J. Nye, M. E. Yount, and J. A. Dumoulin (1998), Catalog of the historically active volcanoes of Alaska, *U.S. Geol. Surv. Open File Rep.*, 98-582, 104 p. [Available at <http://pubs.er.usgs.gov/publication/ofr98582>.]
- Moran, S., O. Kwon, T. Masterlark, and Z. Lu (2006), On the absence of InSAR-detected volcano deformation spanning the 1995–1996 and 1999 eruptions of Shishaldin Volcano, Alaska, *J. Volcanol. Geotherm. Res.*, 150(1–3), 119–131, doi:10.1016/j.jvolgeores.2005.07.013.
- Pallister, J., D. Schneider, J. Griswold, R. Keeler, W. Burton, C. Noyles, C. Newhall, and A. Ratdomopurbo (2013), Merapi 2010 eruption—Chronology and extrusion rates monitored with satellite radar and used in eruption forecasting, *J. Volcanol. Geotherm. Res.*, 261, 144–152, doi:10.1016/j.jvolgeores.2012.07.012.
- Pinel, V., M. P. Poland, and A. Hooper (2014), Volcanology: Lessons learned from synthetic aperture radar imagery, *J. Volcanol. Geotherm. Res.*, 289, 81–113, doi:10.1016/j.jvolgeores.2014.10.010.
- Poland, M. (2014), Time-averaged discharge rate of subaerial lava at Kilauea Volcano, Hawai‘i, measured from TanDEM-X interferometry: Implications for magma supply and storage during 2011–2013, *J. Geophys. Res. Solid Earth*, 119, 5464–5481, doi:10.1002/2014JB011132.
- Poland, M. P., and Z. Lu (2008), Radar interferometry observations of surface displacements during pre- and co-eruptive periods at Mount St. Helens, Washington, 1992–2005, *A Volcano Rekindled: The Renewed Eruption of Mount St. Helens, 2004–2006*, U.S. Geol. Surv. Prof. Pap., 1750, edited by D. R. Sherrod, W. E. Scott, and P. H. Stauffer, chap. 18, pp. 361–382.
- Puglisi, G., A. Bonforte, A. Ferretti, F. Guglielmino, M. Palano, and C. Prati (2008), Dynamics of Mount Etna before, during, and after the July–August 2001 eruption inferred from GPS and differential synthetic aperture radar interferometry data, *J. Geophys. Res.*, 113, B06405, doi:10.1029/2006JB004811.
- Salzer, J., M. Nikkhou, T. Walter, H. Sudhaus, G. Reyes-Dávila, M. Bretón, and R. Arámbula (2014), Satellite radar data reveal short-term pre-explosive displacements and a complex conduit system at Volcán de Colima, Mexico, *Front. Earth Sci.*, 2, 1–11, doi:10.3389/feart.2014.00012.
- Schaefer, L., Z. Lu, and T. Oommen (2015), Dramatic volcanic instability revealed by InSAR, *Geology*, 43(8), 743–746, doi:10.1130/G36678.1.
- Voight, B., and D. Elsworth (2000), Instability and collapse of hazardous gas-pressurized lava domes, *Geophys. Res. Lett.*, 27(1), 1–4, doi:10.1029/1999GL008389.
- Voight, B., R. Sparks, A. D. Miller, R. C. Stewart, R. P. Hoblitt, A. Clarke, J. Ewart, W. P. Aspinall, B. Baptie, and E. S. Calder (1999), Magma flow instability and cyclic activity at Soufriere Hills Volcano, Montserrat, British West Indies, *Science*, 283(5405), 1138–1142, doi:10.1126/science.283.5405.1138.
- Wadge, G., P. Cole, A. Stinton, J.-C. Komorowski, R. Stewart, A. C. Toombs, and Y. Legendre (2011), Rapid topographic change measured by high-resolution satellite radar at Soufriere Hills Volcano, Montserrat, 2008–2010, *J. Volcanol. Geotherm. Res.*, 199(1), 142–152.
- Walter, T., D. Legrand, H. Granados, G. Reyes, and R. Arámbula (2013a), Volcanic eruption monitoring by thermal image correlation: Pixel offsets show episodic dome growth of the Colima volcano, *J. Geophys. Res. Solid Earth*, 118, 1408–1419, doi:10.1002/jgrb.50066.
- Walter, T., A. Ratdomopurbo, S. Subandriyo, N. Aisyah, K. Brotopuspito, J. Salzer, and B. Lühr (2013b), Dome growth and coulée spreading controlled by surface morphology, as determined by pixel offsets in photographs of the 2006 Merapi eruption, *J. Volcanol. Geotherm. Res.*, 261, 121–129, doi:10.1016/j.jvolgeores.2013.02.004.
- Wang, T., and S. Jónsson (2015), Improved SAR amplitude image offset measurements for deriving three-dimensional coseismic displacements, *IEEE J. Sel. Top. Appl. Earth Obs. Remote Sens.*, 18, 1–8, doi:10.1109/JSTARS.2014.2387865.
- Wang, T., S. Jónsson, and R. Hanssen (2014), Improved SAR image coregistration using pixel-offset series, *IEEE Geosci. Remote Sens. Lett.*, 11(9), 1465–1469, doi:10.1109/LGRS.2013.2295429.
- Wicks, C., J. Llera, L. Lara, and J. Lowenstern (2011), The role of dyking and fault control in the rapid onset of eruption at Chaiten volcano, Chile, *Nature*, 478(7369), 374–377, doi:10.1038/nature10541.